Materials Science & Engineering A 710 (2018) 206–213

Contents lists available at ScienceDirect

Materials Science & Engineering A

journal homepage: www.elsevier.com/locate/msea

Deformation of extruded ZK60 magnesium alloy under uniaxial loading in different material orientations

Ying Xiong[a], Qin Yu[b,1], Yanyao Jiang[b,*]

[a] College of Mechanical Engineering, Zhejiang University of Technology, Hangzhou, Zhejiang 310032, China
[b] University of Nevada, Reno, Department of Mechanical Engineering, Reno, NV 89557, USA

ARTICLE INFO

Keywords:
Magnesium alloy
Strain hardening
Twinning
Material orientation

ABSTRACT

The deformation behavior of an extruded ZK60 magnesium (Mg) alloy was investigated experimentally under uniaxial loading in the extrusion direction (ED) and the transverse direction (TD). X-Ray diffractometer (XRD) and electron back scattered diffraction (EBSD) were employed to examine the microstructure evolution using companion specimens. The results indicated that the flow stress and strain hardening rate were strongly affected by the loading directions relative to the initial material orientations. Strong tension-compression asymmetry was exhibited when the loading was applied along the ED. Practically identical stress-strain responses were obtained when the tension/compression was applied in the TD. The difference in tension-compression responses between the ED and TD specimens arises from the distinctive twinning activities, which are inherently related to the initial basal texture. When loading was applied in the ED, copious tension twinning can attained only under compression. However, in the TD, either tension or compression can impose similar amounts of grains under *c*-axis tension, thus activating tension twinning in both directions. Detailed analyses of strain hardening rate responses under different loading paths were made. The deformation mechanisms associated with different stages of strain hardening rate were discussed with a particular emphasis on the roles of deformation twinning.

1. Introduction

Magnesium (Mg) alloys are regarded as promising structural materials in the transportation industry by virtue of their low density and high specific strength. However, strong texture is developed in wrought Mg alloys treated by typical thermomechanical processing, such as extrusion and rolling [1]. Therefore, the loading direction relative to the initial texture has a significant effect on the mechanical properties of wrought Mg alloys [2–4].

For wrought Mg alloys, the *c*-axes of the grains are perpendicular to the extrusion direction (ED) or rolled direction (RD) and, therefore, $\{10\bar{1}2\}$ tension twinning occurs during compressive loading along the ED or RD. The effects of $\{10\bar{1}2\}$ tension twinning on the deformation behavior (flow stress and strain hardening) of wrought Mg alloys have been investigated in many studies [2–9]. There exist different views regarding the role of tension twinning on the strain hardening behavior. Three mechanisms have been proposed: Hall–Petch effect, texture hardening, and Basinski mechanism. The Hall-Petch effect arises from segmentation of twinned grains [7]. Twinning-induced grain refinement may cause the twin boundaries acting as barriers to dislocation slips and thus increasing the strain hardening rate. Texture hardening is a result from reorientation of crystal lattice caused by twinning [4,10]. The lattice reorientation of *c*-axes by 86° can cause the grains to rotate toward hard orientation and hence enhance the strain hardening rate. The Basinski mechanism comes from a glissile-to-sessile transformation [11]. The transformation of glissile dislocation into sessile dislocations within the twin interiors causes an increase in the strain hardening rate.

Aside from mechanical twinning, dislocation slips always accompany and act as an essential deformation mode for plastic deformation of Mg alloys. Basal $< a >$ slip, prismatic $< a >$ slip, and pyramidal $< c + a >$ slips, as well as $\{10\bar{1}2\}$ tension twinning and $\{10\bar{1}1\}$ compression twinning [8,12–14], are collectively operated and contribute to the plastic deformation. Previous studies have shown that the relative activities of different deformation modes are governed by factors such as temperature [7,15], strain rate [16,17], and grain size [8,18].

Structural components made from Mg alloys can be subjected to loading in different directions relative to the original material texture. The twin morphology, twin volume fraction, and texture can be varied in response to different loading directions [9]. It is important to explore the deformation behavior of Mg under different loading paths and to

* Corresponding author.
E-mail address: yjiang@unr.edu (Y. Jiang).
[1] Current address: Schlumberger-Doll Research Center, One Hampshire St, Cambridge, MA 02139, USA.

http://dx.doi.org/10.1016/j.msea.2017.10.059
Received 18 July 2017; Received in revised form 11 October 2017; Accepted 19 October 2017
Available online 22 October 2017

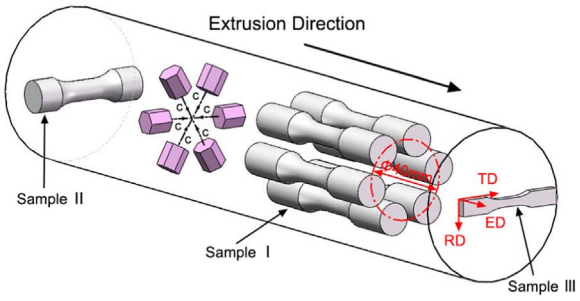

Fig. 1. Schematic of specimen geometries and sizes, and their orientations relative to the initial texture.

understand the associated deformation mechanisms. In the present study, the stress-strain responses were obtained from an extruded ZK60 Mg alloy loaded in two different material orientations. The correlation between the microstructure evolution and the strain hardening rate was investigated. The role of deformation twins on material's strain hardening was elucidated.

2. Material and experiments

2.1. Material and specimen

The material used in the present study is an extruded ZK60 (5 wt% Zn, 0.64 wt% Zr, Mg balance) Mg alloy. Dog-bone shaped testing specimens were machined from the material bar with a diameter of 76 mm, as shown in Fig. 1. Monotonic tension and monotonic compression experiments along the ED were carried out using Sample I geometry. Six cylindrical testing specimens distribute uniformly on a circle on the TD-RD plane. Each Sample I specimen has a gage length of 15 mm and a diameter of 10 mm within the gage section. Monotonic compression and monotonic tension experiments along the traverse direction (TD) were conducted using samples II and III geometries, respectively. The cylindrical Sample II has a gage length of 15 mm and a diameter of 10 mm within the gage section, and the plate Sample III has a gage section of 8 mm × 4 mm × 4 mm. Before mechanical testing, the outer surface of the specimen within the gage section was polished using silicon carbide papers with grit numbers ranging from 240 to 1500.

2.2. Experiments

Monotonic loading experiments were conducted in ambient air using servo-hydraulic material testing systems. In order to clarify the microstructure evolution during mechanical deformation, tests were interrupted at different strains. In the ED, companion specimens were compressed to 3%, 9%, and 13.2% (fracture). Under tension, the specimens were loaded to 5% and 20.1% (fracture). In the TD, the cylindrical specimens were compressed to 12.9% (fracture). For tension in the TD, the plate specimens were extended to 1%, 7%, and 13.8% (fracture). All the experiments were conducted at a strain rate of approximate 6.0×10^{-3} /s. True stress and true strains are reported and presented.

The microstructures of the initial and deformed samples were measured on the TD-RD plane (Samples I and III) using X-Ray diffractometer (XRD). Nucleation of $\{10\bar{1}2\}$ tension twin can make the basal plane rotate from the ED to a direction perpendicular to ED. The

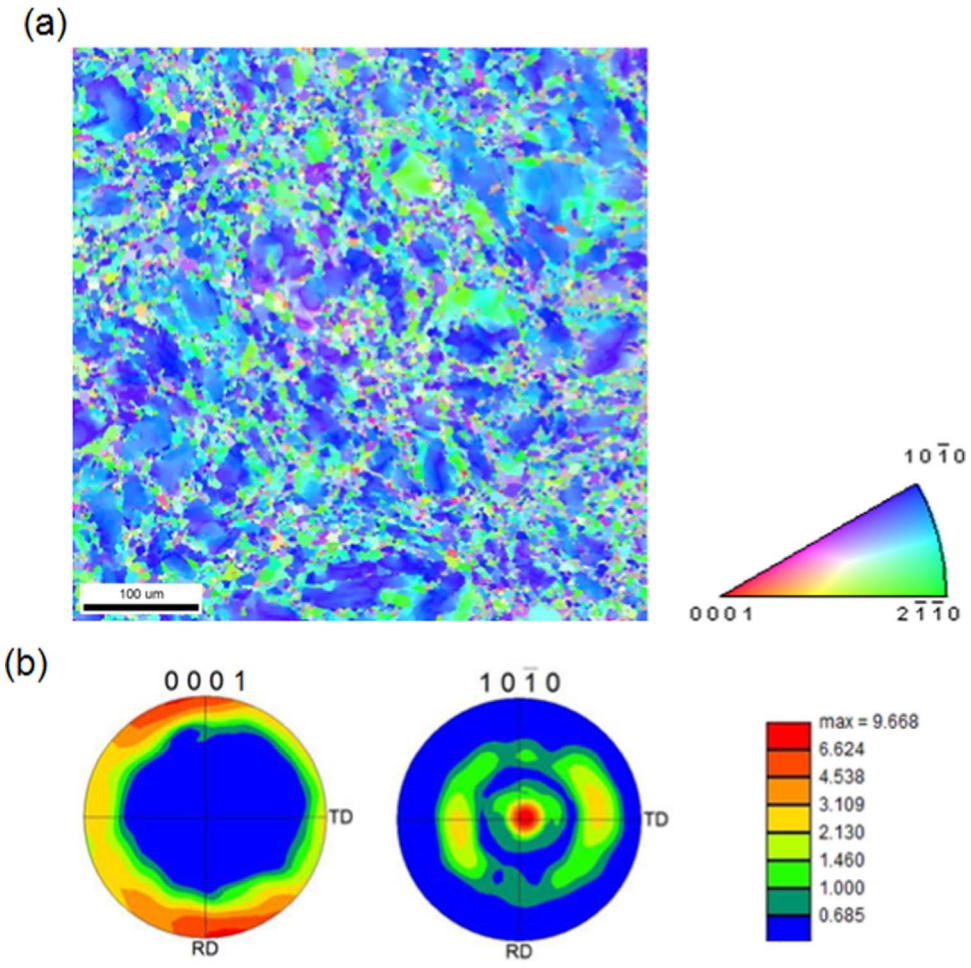

Fig. 2. Initial microstructure and texture of extruded ZK60 magnesium alloy characterized by EBSD: (a) microstructure and (b) (0002) and $\{10\bar{1}0\}$ pole figures.

degree of tension twinning remained in the specimens was evaluated by analyzing the scanned XRD pattern. The degree of twins can be represented by the inverse value of $\lambda = \frac{I_{(0002)}}{I_{(0002)} + I_{(10\bar{1}0)}}$ using the integrated intensity of $\{10\bar{1}0\}$ and (0002) peaks, where the parameter λ of the deformed samples is further normalized by the λ-value of the initial material, and the normalized λ value is denoted by λ_{Norm} [19].

For the fractured ED specimens (Sample I), electron back scattered diffraction (EBSD) examination was conducted on the polished TD-RD plane that is 5 mm away from the macroscopic fracture surface. All the EBSD scans were conducted on an area of 200 μm × 200 μm with a step size of 0.5–0.8 μm. The acceleration voltage was set at 20 KeV to acquire the indexable Kikuchi diffraction pattern. The raw EBSD data was acquired by EDAX-TSL OIM Data Collection System. OIM Analysis v7 package was used to post-process the raw data. The EBSD raw data was cleaned up by applying the "Grain Confidence Index (CI) Standardization" and "Dilation" methods. Special attention was paid when applying the "Dilation" method. The orientation maps before and after dilation were carefully compared to prevent any incorrect change of the microstructure.

3. Results and discussion

3.1. Initial microstructure and texture of material

Fig. 2 shows the initial microstructure of the extruded ZK60 Mg alloy measured by EBSD. The initial microstructure observed on the TD-RD plane shows a mixture of large grains with an average width of 50 μm and clusters of recrystallized grains with average size of 8 μm [20]. No tension twins were found at the untested state (Fig. 2 a). The (0002) and $\{10\bar{1}0\}$ pole figures presented in Fig. 2b indicate that the material exhibits a typical basal fiber texture, i.e. the basal planes are parallel to the ED. Further revealed from Fig. 2b, the *c*-axes of a majority of grains are perpendicular to the ED and, in particular, most of the *c*-axes are "randomly" distributed within the TD-RD plane, which is perpendicular to the ED. To visualize the initial texture, a schematic of hexagonal close packed (hcp) unit cells that represent different crystal orientations in the initial material is embedded in Fig. 1.

3.2. Deformation in the ED

3.2.1. Macroscopic mechanical behavior

The true stress–true strain curves and the corresponding strain hardening rate curves under compressive and tensile loading along the ED are presented in Fig. 3a and b, respectively. From Fig. 3a, the ED samples exhibit typical tension-compression asymmetry. The tensile flow curve shows a typical concave-down shape, while the compressive flow curve reveals a sigmoidal shape. The compressive yield stress (~158 MPa) is obviously lower than the tensile yield stress (~277 MPa), whereas the compressive fracture stress (~485 MPa) is much higher than the tensile fracture stress (~372 MPa). The compressive and tensile strains at fracture are 13.2% and 20.1%, respectively.

The strain hardening rate curves are plotted in Fig. 3b. Under compression, the strain hardening rate curve can be divided into four stages: (i) Stage I, an initial decreasing hardening rate before ~0.5% strain, (ii) Stage II, a slowly increasing hardening rate from ~0.5% to ~5% strain, (iii) Stage III, a fast increasing hardening rate from ~5% to ~7.5% strain, and (iv) Stage IV, a decreasing hardening rate from ~7.5% stain to compressive rupture. The strain hardening rate curve under the tensile loading can be divided into two stages. A point of inflection appears at ~1% strain, the hardening rate rapidly decreases before the point, and slowly decreases after the point with increasing strain. The results show that the compressive and tensile deformation mechanisms are different at different strain levels.

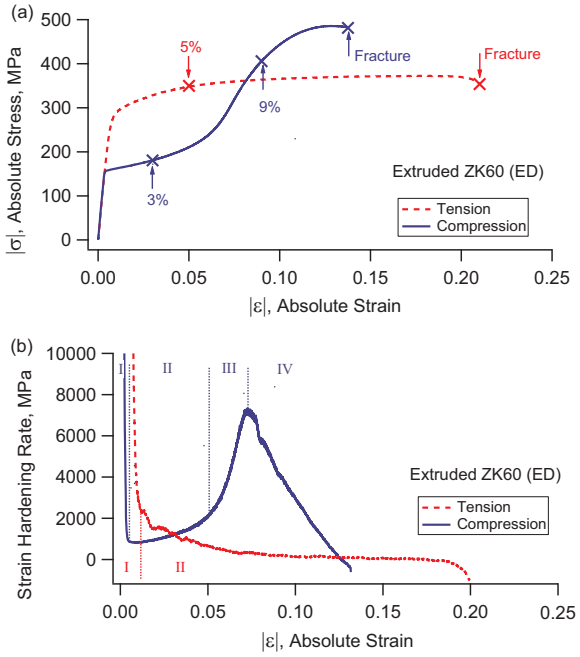

Fig. 3. Mechanical responses of extruded ZK60 alloy loaded along the ED: (a) stress-strain curves, and (b) strain hardening rate curves.

3.2.2. Microstructure evolution

The plastic deformation of the material causes the development of crystallographic texture, and it will change the diffraction intensity of the basal planes. The XRD patterns scanned on the TD-RD plane of the samples at different strain levels are shown in Fig. 4 for compression loading and tension loadings, respectively. The degree of $\{10\bar{1}2\}$ tension twinning can be qualitatively evaluated by the parameter λ_{Norm}. A higher λ_{Norm} indicates a higher twin volume fraction. Under the compressive loading (Fig. 4a), the value of λ_{Norm} increases significantly from 1 up to 21.4 after ~3% strain. This suggests that the $\{10\bar{1}2\}$ tension twins have nucleated and grown even at a relatively small compressive

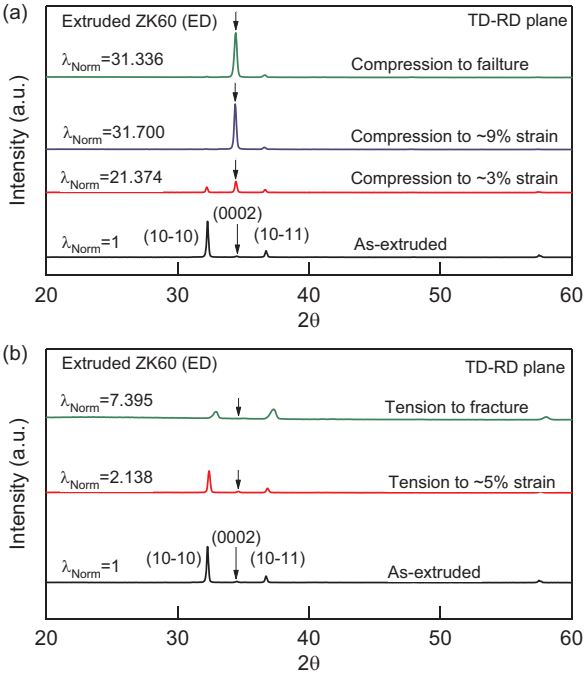

Fig. 4. XRD patterns of extruded ZK60 Mg alloy after (a) compressive and (b) tensile loading at different strain levels along the ED.

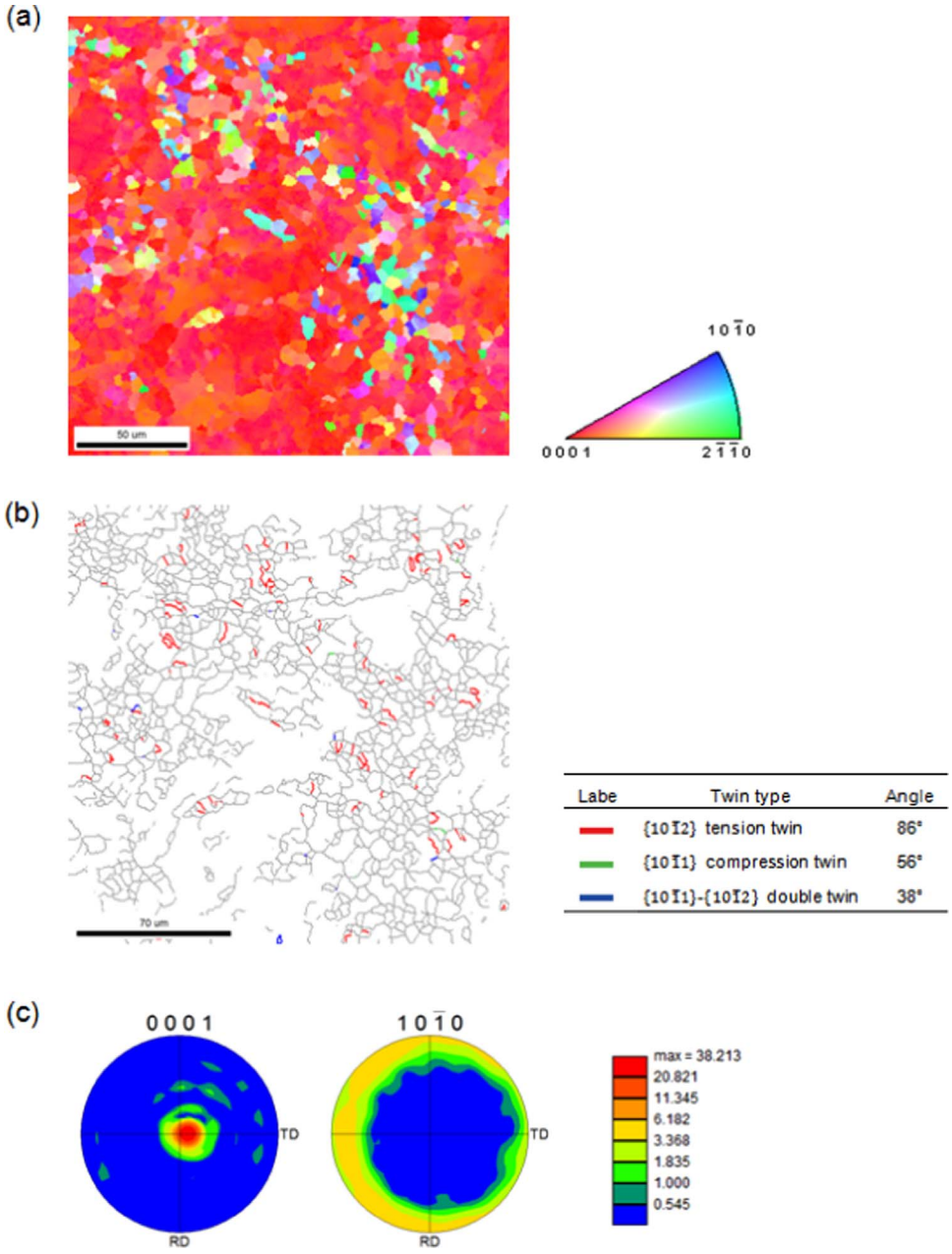

Fig. 5. Microstructure and texture characterized by EBSD after compression fracture in the ED: (a) inverse pole figure map; (b) grain and twin boundary map; (c) pole figures.

strain of 3%. When the compressive strain increases to ~9%, the value of λ_{Norm} continuously increases to 31.7, and then λ_{Norm} is 31.3 at the fracture of the specimen. It is speculated that twinning growth is exhausted between 3% and 9% strain, while the deformation mechanism before compression fracture can be more complicated. Previous studies suggest that the multiple {10$\bar{1}$2} twin variants would be formed in this strain range [11,21,22]. In the tensile loading (Fig. 4b), the value of λ_{Norm} increases slightly from 1 to 2.1 when the strain increases to 5%, and continuously rises to 7.4 until fracture. While tension along the ED does not favor copious tension twinning, small amount of {10$\bar{1}$2} tension twins is likely to be activated to accommodate the mismatched plastic deformation between neighboring grains [8].

To identify the deformation mechanism at fracture, EBSD scans were made on the polished TD-RD surface away from the macroscopic fracture surface for both tension and compression specimens. The results are shown in Figs. 5 and 6, respectively. As seen from Fig. 5a, very few twin boundaries are observed in the large sized grains after compression fracture along the ED. This is caused by the coalesce of growing twin boundaries [6]. {10$\bar{1}$2} twinning boundaries can be better identified in the small sized grains (Fig. 5b). In addition, a few {10$\bar{1}$1} compression twins and some {10$\bar{1}$1}-{10$\bar{1}$2} double twins are observed. Combining with the XRD results (Fig. 4a), it is derived that most of the original material is twinned as the sample is compressed to ~9% strain. Before fracture in compression, the significant decrease of the twinning boundaries is due to the growth and coalescence of tension twinning. The slight decrease of {10$\bar{1}$2} twin volume fraction can be attributed to the activation of {10$\bar{1}$1} compression twins and {10$\bar{1}$1}-{10$\bar{1}$2} double twins in the twinned grains [23]. This result is consistent with observations in earlier reports [7,24]. The behavior of tension twinning during compressive deformation can also be verified by texture evolution. The *c*-axes of the grains in the initial material are perpendicular to the ED (Fig. 2b). During compressive deformation, {10$\bar{1}$2} tension twinning is activated so that the *c*-axes of these crystals are reoriented parallel to the ED. The {0002} pole figures show that the maximum value of multiples of random (mrd) density in the fractured sample, 38.2, (see Fig. 5c) is much higher than that in the initial material, 9.7

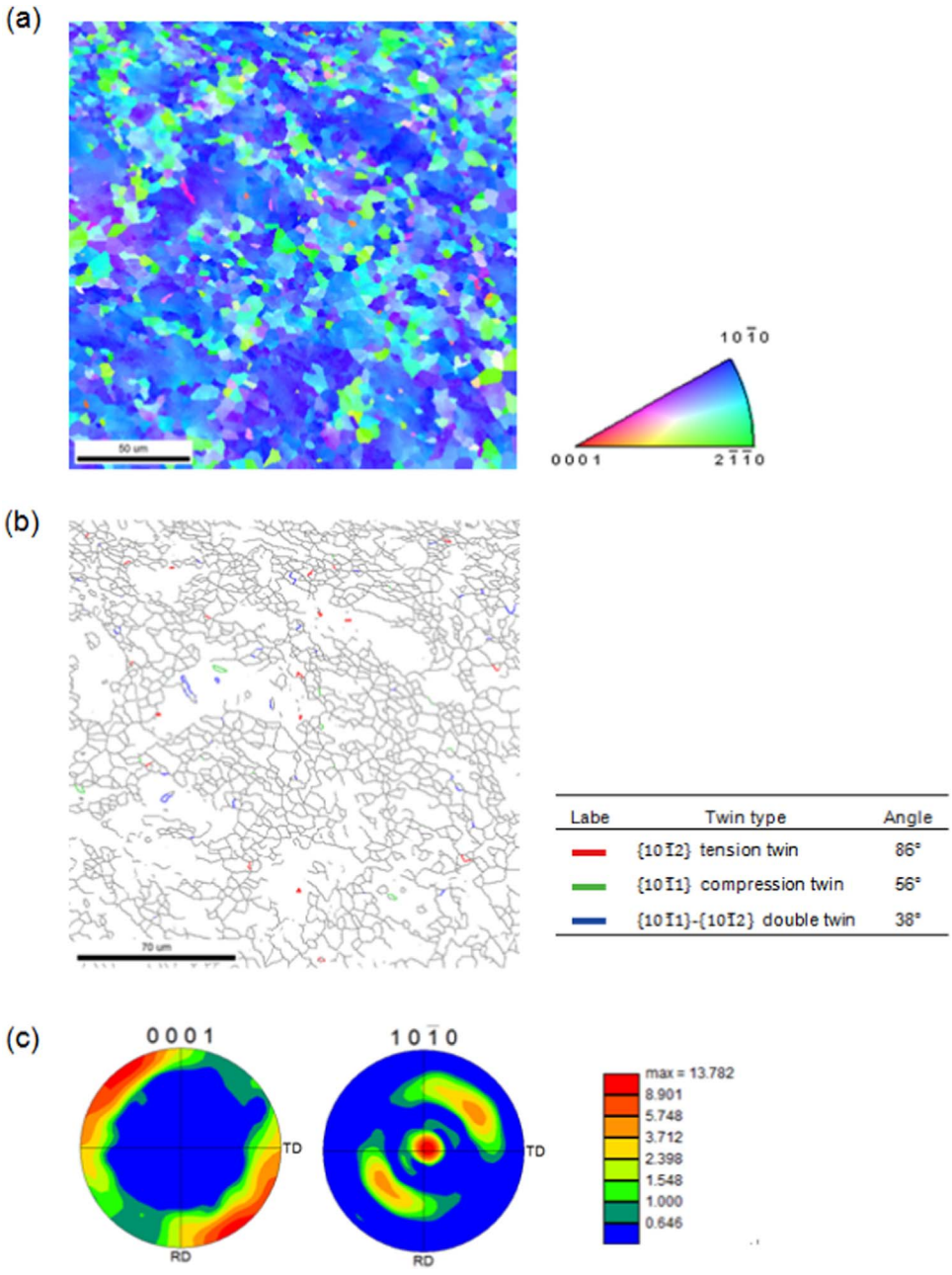

Fig. 6. Microstructure and texture characterized by EBSD after extension fracture in the ED: (a) inverse pole figure map; (b) grain and twin boundary map; (c) pole figures.

(see Fig. 2b). The observed microstructure and texture results are consistent with those reported by Dong et al. [24] who pointed out that {10$\bar{1}$1}-{10$\bar{1}$2} double twinning occurred in large deformation stage for an extruded ZK60 Mg alloy and the number of twins increased greatly when the testing specimen was compressed to 10% strain along the ED. Compared to the materials used in the current study, the grain size of the extruded ZK60 Mg alloy reported in Ref. [24] is similar, but the mrd density of the initial texture is higher (14.2) and the strain rate is higher (1.33×10^{-2}/s). The initial texture and the strain rate may affect the degree of activation of {10$\bar{1}$1}-{10$\bar{1}$2} double twinning [24]. Therefore, the capacity of {10$\bar{1}$1}–{10$\bar{1}$2} double twinning in the present study is less than that reported in Ref. [24] due to a lower texture density and a slower strain rate.

EBSD results of tensile fracture sample are shown in Fig. 6. The microstructure of the fractured sample along the ED is similar to that of the original material (Fig. 6a). However, a few {10$\bar{1}$2} tension twins are present in the larger grains. In addition, a few {10$\bar{1}$1} compression twins and some {10$\bar{1}$1}–{10$\bar{1}$2} double twins are observed in Fig. 6b. The tensile loading imposes *c*-axis compression on the original material, which favors the formation of {10$\bar{1}$1} compression twins and {10$\bar{1}$1}–{10$\bar{1}$2} double twins. The excessive shearing caused by double twinning may cause microcracking at double twin boundaries, and may lead to tensile fracture [25].

3.2.3. Deformation mechanisms

Four stages are exhibited in the compressive strain hardening curve (Fig. 3b). When the compression strain reaches approximate 0.5%, the material yields macroscopically. This is due to nucleation of {10$\bar{1}$2} tension twins (CRSS = ~2–5 MPa). The occurrence of tension twinning effectively releases the stress concentration during deformation [26], leading to a rapid decrease in the strain hardening rate (Stage I). With further straining to ~5% (Stage II), fresh tension twins are nucleated successively in a number of grains. Due to the fact that twinning rotates grains from soft to hard orientations, texture hardening takes effect during Stage II, leading to slow strain hardening (Fig. 3b) [6,26]. In the strain range between ~5% and ~7.5% (Stage III), XRD and EBSD

results indicate that a high density of {10$\bar{1}$2} tension twins exists during this period. On one hand, the large number of twin boundaries act as barriers to dislocation motion, and thus enhancing the strain hardening rate [6]. On the other hand, twin-twin interaction resulted from multiple {10$\bar{1}$2} twin variants may occur in some grains [21,22]. A {10$\bar{1}$2} tension twin variant nucleated earlier provides an effective barrier to the impingement of latter formed {10$\bar{1}$2} twin variant, thus further enhancing the strain hardening rate [9,11,21,22]. In short, the higher strain hardening rate in Stage III (Fig. 3b) can be attributed to the enhanced activities of twin-slip interaction and twin-twin interaction. At a strain of approximate 7.5%, the tension twins consume almost the entire grains. As a result, most of the c-axes in these grains are parallel to the loading direction. To accommodate further compression, pyramidal < c+a > slips (CRSS = ~35–80 MPa) might be activated. {10$\bar{1}$1} compression twins (CRSS = ~30–100 MPa) and {10$\bar{1}$1}–{10$\bar{1}$2} double twins might form in the primary {10$\bar{1}$2} tension twins [7,19,20]. {10$\bar{1}$1} compression twinning and {10$\bar{1}$1}–{10$\bar{1}$2} double twinning have an effect of rotating the basal planes towards a more favorable orientation for basal slips, which likely leads to a pronounced decrease in the strain hardening rate during Stage IV [15,27,28].

Comparing the stress-strain response under tension with that under compression (Fig. 3a), it is found the tensile yield stress (277 MPa) is higher than the compressive yield stress (158 MPa). In addition, the strain hardening rate under tension displays a persistently decreasing trend (Fig. 3b). As indicated from the initial texture (Fig. 2), the (0002) planes of most grains are parallel to the tensile axis and therefore, tension twinning is difficult to be activated. Instead, the macro tensile yielding is likely caused by the prismatic < a > slips with a higher CRSS [16]. Once the stress is beyond the macro yielding point, pyramidal < c+a > slip might be activated to accommodate further plastic strain. Additionally, a few {10−11} compression twins and some {10−11}–{10−12} double twins might be nucleated. The grain reorientation led by these two twinning modes is beneficial to the activation of basal < a > slips, which contributes to a continuous decrease in the strain hardening rate until the final fracture.

3.3. Deformation in the TD

3.3.1. Macroscopic mechanical behavior

Fig. 7 shows the true stress–true strain curves and the corresponding hardening rates under the compressive and tensile loading along the TD. From Fig. 7a, it is found that the stress-strain responses obtained under the compression and tension are similar. Both stress-strain curves show a concave-down shape. The compressive yield stress (~147 MPa) is close to the tensile yield stress (~132 MPa), and the compressive fracture stress (~348 MPa) and the tensile fracture stress (~340 MPa) are practically identical. The compressive and tensile fracture strains are 12.9% and 13.8%, respectively. It can be seen from Fig. 7b that the strain hardening rate curves can be divided into three stages. The strain hardening rate continually decreases before ~1% strain (Stage I). However, the hardening rate curve exhibits a plateau characteristic up to ~5% strain (Stage II), during which the strain hardening rate remains almost constant. Once exceeding ~5% strain, the strain hardening rate decreases persistently until fracture of the specimen (Stage III).

3.3.2. Microstructure evolution

Fig. 8 shows the scan patterns measured by XRD on the TD-RD plane of the TD samples tensioned to different strain levels. When the tensile strain increases to ~1%, the value of λ_{Norm} is measured to be 0.97, which is very close to the λ_{Norm} value (1) of the original material. Such a trivial difference of λ_{Norm} is not sufficient to detect the change of texture. It can be speculated that the aggregate grain orientation of the material at 1% strain remains the same as the original material. Beyond 1% strain, the value of λ_{Norm} rises to 8.01 when the strain increases to ~7%, and then increases to 15.94 at the fracture of the specimen. The

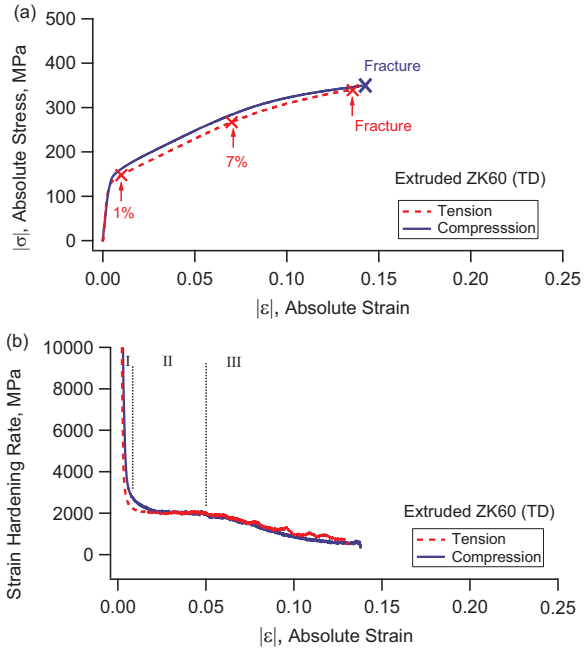

Fig. 7. Mechanical responses of extruded ZK60 Mg alloy loaded along the TD: (a) stress-strain curve, and (b) strain hardening rate curve.

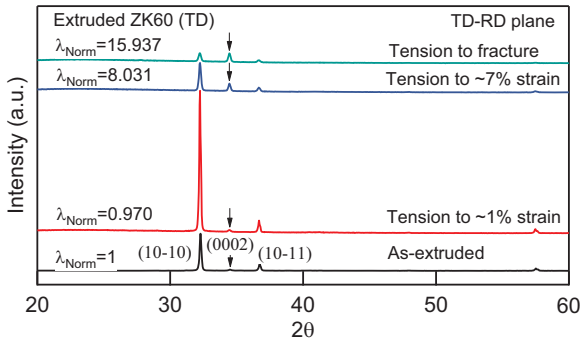

Fig. 8. XRD patterns of extruded ZK60 alloy after tensile loading at different strain levels along the TD.

clear rise of λ_{Norm} signifies {10$\bar{1}$2} tension twinning occurs in a few grains which are oriented favorably for tension twinning after ~1% strain. It is noted that when the material is almost completely twinned at the compression fracture in the ED, the λ_{Norm} value is ~31 (see Fig. 4b). A λ_{Norm} value of ~16 in the TD specimen at tension fracture suggests that approximately a half of the original material is twinned in the TD specimen when it is tensioned to fracture.

3.3.3. Deformation mechanism

As characterized from Fig. 2b and illustrated in Fig. 1, most of the *c*-axes in the original extruded ZK60 is "randomly" distributed within the TD-RD plane and perpendicular to the ED. For the TD specimens, the loading direction is oriented within the TD-RD plane so that various slip/twinning deformation modes can be activated during plastic deformation under compressive or tensile loading. The CRSS values of prismatic < *a* > slip, pyramidal < *c*+*a* > slip and {10$\bar{1}$1} compression twinning are higher than those of basal < *a* > slip and {10$\bar{1}$2} tension twinning and therefore, basal < *a* > slip and {10$\bar{1}$2} tension twinning are favorable to be activated during compressive or tensile loading. Additionally, the CRSS of basal < *a* > slip (CRSS = ~0.5 MPa) is lower than that of {10$\bar{1}$2} tension twinning, thus basal < *a* > slip is activated earlier than is {10$\bar{1}$2} tension twinning. In this case, the plastic deformation in the early stage (Stage I) is dominated by basal < *a* > slip

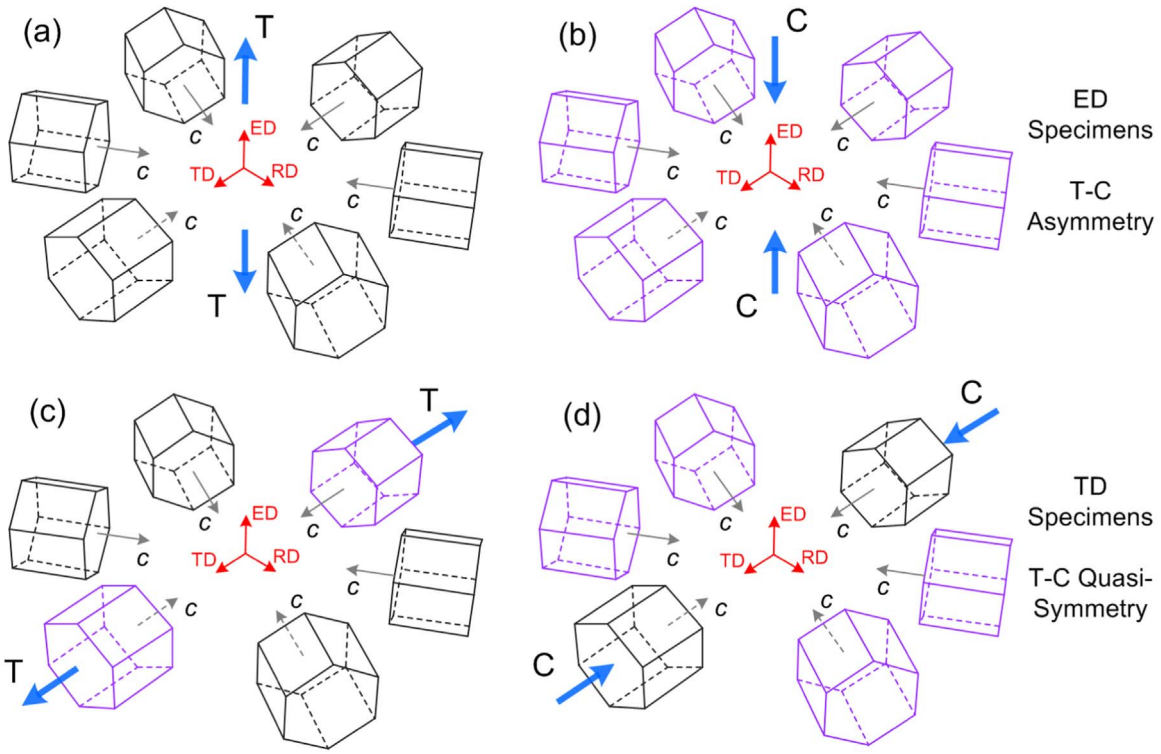

Fig. 9. Schematic illustration of tension twinning activities in different oriented grains under different loading conditions (black-colored unit cells: no twinning; violet-colored unit cells: twinning possible): (a) tension along the ED, (b) compression along the ED, (c) tension along the TD, and (d) compression along the TD.

during compressive or tensile loading, leading to a rapid decrease in the strain hardening rate with increasing strain.

During Stage II deformation which ranges from the macro yield point up to ~5%, a plateau of strain hardening rate is exhibited in the TD specimens under both tension and compression. An increase in λ_{Norm} measured by XRD (Fig. 8) clearly indicates that $\{10\bar{1}2\}$ tension twins are operated during this Stage. Unlike the ED specimen, where tension twinning is activated preferably under compression, tension twinning can be activated in TD specimens under both tension and compression. To better explain the twinning behavior in the TD specimen, a schematic illustration is created to demonstrate the tension twinning activities under different loading conditions, as shown in Fig. 9. The grain orientations derived from the initial texture Fig. 2b) are represented by hcp unit cells. In Fig. 9, the *c*-axis of the black-colored unit cells is subjected to compression, i.e. twinning is unlikely to be nucleated in such orientations. On the contrary, tension is imposed on the *c*-axis of the violet-colored unit cells, i.e. these grain orientations favor tension twinning. For TD specimens, loading is applied on the TD-RD plane, where the *c*-axes of grains are "randomly" distributed. Either tension or compression is able to impose *c*-axis tension on some fraction of grains – the "violet unit cells" as demonstrated in Fig. 9c and d. Since the distribution of *c*-axes on the TD-RD plane in the initial texture is not perfectly random, the volume fractions of grains subjected to *c*-axis tension under tension and compression will not be exactly identical. This is likely the reason explaining why the measured stress-strain responses under tension and compression show a slight difference (Fig. 7a).

The experimental observation reveals that the morphology of tension twinning in TD sample is different from that of ED sample under compressive loading [6]. Usually, the tension twins are nucleated at grain boundaries and terminate at the opposite grain boundary [29]. However, the lenticular shape and a wedged tip are totally embedded within the parent matrix in TD sample, which is defined as stopped twins [6]. The formation of stopped twins is likely to induce easier and earlier nucleation of slip dislocations, which would increase the extent of twin-slip interactions during the lengthwise thickening of a twin [6]. Therefore, the plateau observed in the middle stage (Stage II) should be considered as the competition between the stopped twinning and twin-slip interaction. During Stage III, tension twinning continues as evidenced by the XRD measurement (Fig. 8). Meanwhile, $\{10-11\}$ compression twining and $\{10-11\}$-$\{10-12\}$ double twinning are likely to be nucleated due to the increased stress level. The activation of compression twins and double twins is responsible for the decreasing strain hardening rate during Stage III plastic deformation [6].

4. Further discussion

The current study confirms that the behavior of strain hardening rate is significantly affected by the loading direction with respect to the initial material orientation. Previous studies have indicated that twins play an important role in strain hardening behavior [2–9]. The current study reveals further microstructural factors that can affect the twinning behavior and consequently determine the variance of strain hardening rate.

1) Grain-size inhomogeneity. Taking the compressive deformation of the material loaded along the ED as an example, previous research indicates that the strain hardening curves in extruded AZ31 and AM30 Mg alloys are divided into three regimes [5,10]. Before the macro yielding, the strain hardening rate decreases rapidly (Stage I), then the rate indicates a distinct increase followed by a sharp decrease (Stages II and III, respectively). However, in the present work, the strain hardening rate curve after the yield point consists of a slightly increased slope (Stage II) and a sharply increased slope (Stage III), followed by a reduced slope (Stage IV). The extruded ZK60 Mg alloy studied in this paper is composed of elongated large grains and equiaxed fine grains [20]. At the early stage of plastic deformation, $\{10\bar{1}2\}$ tension twins nucleate and grow in the *large* grains, and the hardening behavior of Stage II (see Fig. 3b) can be ascribed to the effect of twinning-induced 86° grain rotation to a

"hard" orientation. In this case, the material undergoes an uneven plastic deformation, and as a result, the strain hardening rate increases slowly with straining. As the strain increases from 5% to 7.5%, $\{10\bar{1}2\}$ tension twinning is observed in the *small-sized* grains and multiple $\{10\bar{1}2\}$ twin variant may be formed in some grains in addition to re-rotation of the crystal that causes the activation of slip systems. Therefore, the twin-slip and twin-twin interactions lead to the increment of strain hardening rate in Stage III (see Fig. 3b). In summary, the hardening effect introduced by $\{10\bar{1}2\}$ tension twinning arises from two deformation mechanisms: texture hardening and the Hall–Petch effect, with the latter being more obvious in the inhomogeneous microstructure.

2) Initial texture. Comparing the TD samples with the ED samples (Figs. 3 and 7), it can be found that the strain hardening rate of the ED sample under compressive loading is lower than that of the TD sample at Stage II, and the length of Stage II in TD sample is shorter than that in the ED sample. With the same plastic deformation in Stage II, more $\{10\bar{1}2\}$ tension twinning occurs in the ED sample comparing with the TD sample (Figs. 4 and 8). This is because the volume fraction of grains which are favorable for $\{10\bar{1}2\}$ tension twinning in the ED sample is higher than that in TD sample. Accordingly, the number of twinning-induced 86° grain rotation to "hard" orientation in the ED sample is higher than that in the TD sample. This is a probable reason why the strain hardening rate of the ED sample is lower than that of the TD sample in Stage II. The length of Stage II is determined by the volume fraction of $\{10\bar{1}2\}$ tension twinning.

5. Conclusions

Deformation and microstructure under different loading directions with respect to the initial material orientation were investigated for an extruded ZK60 Mg alloy. Major conclusions are summarized as follows.

(1) The true stress-strain curves and the corresponding strain hardening rates under compressive and tensile loading along the extruded direction (ED) show a strong anisotropy. The variations of strain hardening rates can be divided into four stages in the compressive loading, whereas there are two stages in the tensile loading.
(2) When compressed along the ED, significant $\{10\bar{1}2\}$ tension twinning occurs during the early stage of deformation (~7.5% strain). Tension twinning induced strain hardening is dominated by two deformation mechanisms, namely, texture hardening and Hall–Petch effect. Twinning-induced 86° grain reorientation to "hard" orientation dominants the hardening behavior of Stage II. Twinning-induced barriers to dislocation movement dominants the hardening behavior in Stage III. When the strain exceeds ~7.5%, several competitive deformation mechanisms accommodate the plastic strain in Stage IV.
(3) For the tensile loading along the ED, prismatic $< a >$ slips dominate the macro yield deformation at the early stage (~1% strain). The decreasing strain hardening rate observed at a latter stage in the tensile (Stage II) and compressive (Stage IV) deformation along the ED is mainly attributed to the softening effect induced by $\{10\bar{1}1\}$ compression twinning and $\{10\bar{1}1\}$–$\{10\bar{1}2\}$ double twinning.
(4) The true stress-strain curves and the corresponding strain hardening rates under compressive and tensile loading along the transverse direction (TD) show similar features with a tension-compression symmetry. Basal $< a >$ slips dominant the hardening behavior of Stage I while $\{10\bar{1}2\}$ tension twinning is involved in the hardening behavior of Stage II where a plateau of strain hardening rate is exhibited.

Acknowledgements

The author gratefully acknowledges financial supports provided by the National Natural Science Foundation of China (No. 51775502, 51275472). Yanyao Jiang thanks support from the National Science Foundation (CMMI-1462885).

References

[1] S.R. Agnew, Wrought magnesium: a 21st century outlook, JOM 56 (2004) 20–21.
[2] R. Gehrmann, M.M. Frommert, G. Gottstein, Texture effects on plastic deformation of magnesium, Mater. Sci. Eng. A 395 (2005) 338–349.
[3] X.Y. Lou, M. Li, R.K. Boger, S.R. Agnew, R.H. Wagoner, Hardening evolution of AZ31B magnesium sheet, Int. J. Plast. 23 (2007) 44–86.
[4] M. Knezevic, A. Levinson, R. Harris, R.K. Mishra, R.D. Doherty, S.R. Kalidindim, Deformation twinning in AZ31: influence on strain hardening and texture evolution, Acta Mater. 58 (2010) 6230–6242.
[5] D. Sarker, D.L. Chen, Detwinning and strain hardening of an extruded magnesium alloy during compression, Scr. Mater. 67 (2012) 165–168.
[6] Q. Ma, H. El. Kadiri, A.L. Oppedal, J.C. Baird, B. Li, Horstemeyer, M.F. Vogel, S.C. Twins, effects in a rod-textured AM30 Magnesium alloy, Int. J. Plast. 29 (2012) 60–76.
[7] L. Jiang, J.J. Jonas, A.A. Luo, A.K. Sachdev, S. Godet, Influence of {10-12} extension twinning on the flow behavior of AZ31 Magnesium alloy, Mater. Sci. Eng. A 445–446 (2007) 302–309.
[8] J. Koike, Enhanced deformation mechanisms by anisotropic plasticity in polycrystalline Magnesium alloys at room temperature, Metall. Mater. Trans. A 36 (2005) 1689–1696.
[9] S.G. Hong, S.H. Park, C.S. Lee, Role of {10−12} twinning characteristics in the deformation behavior of a polycrystalline magnesium alloy, Acta Mater. 58 (2010) 5873–5885.
[10] B.S. Wang, R.L. Xin, G.J. Huang, Q. Liu, Effect of crystal orientation on the mechanical properties and strain hardening behavior of magnesium alloy AZ31 during uniaxial compression, Mater. Sci. Eng. A 534 (2012) 588–593.
[11] H.El Kadiri, J. Kapil, A.L. Oppedal, L.G. Hector Jr., S.R. Agnew, M. Cherkaoui, S.C. Vogel, The effect of twin–twin interactions on the nucleation and propagation of $\{10\bar{1}2\}$ twinning in magnesium, Acta Mater. 61 (2013) 3549–3563.
[12] J. Koike, T. Kobayashi, T. Mukai, H. Watanabe, M. Suzuki, K. Maruyama, K. Higashi, The activity of non-basal slip systems and dynamic recovery at room temperature in fine-grained AZ31B magnesium alloys, Acta Mater. 51 (2003) 2055–2065.
[13] M.R. Barnett, Twinning and the ductility of magnesium alloys. Part I: "Tension" twins, Mater. Sci. Eng. A 464 (2007) 1–7.
[14] M.R. Barnett, Twinning and the ductility of magnesium alloys. Part II. "Contraction" twins, Mater. Sci. Eng. A 464 (2007) 8–16.
[15] L. Jiang, J.J. Jonas, R.K. Mishra, A.A. Luo, A.K. Sachdev, S. Godet, Twinning and texture development in two magnesium alloys subjected to loading along three different strain paths, Acta Mater. 55 (2007) 3899–3910.
[16] C.J. Geng, B.L. Wu, X.H. Du, Y.D. Wang, Y.D. Zhang, F. Wagner, C. Esling, Stress–strain response of textured AZ31B magnesium alloy under uniaxial tension at the different strain rates, Mater. Sci. Eng. A 559 (2013) 307–313.
[17] N. Dixit, K.Y. Xie, K.J. Hemker, K.T. Ramesh, Microstructural evolution of pure magnesium under high strain rate loading, Acta Mater. 87 (2015) 56–67.
[18] M.R. Barnett, Z. Keshavarz, A.G. Beer, D. Atwell, Influence of grain size on the compressive deformation of wrought Magnesium –3Al–1Zn, Acta Mater. 52 (2004) 5093–5103.
[19] Y. Xiong, Q. Yu, Y. Jiang, Cyclic deformation and fatigue of extruded AZ31B magnesium alloy under different strain ratios, Mater. Sci. Eng. A 649 (2016) 93–103.
[20] Y. Xiong, Q. Yu, Y. Jiang, An experimental study of cyclic plastic deformation of extruded ZK60 magnesium alloy, Int. J. Plast. 53 (2014) 107–124.
[21] Q. Yu, J. Wang, Y. Jiang, R.J. McCabe, N. Li, C.N. Tomé, Twin–twin interactions in magnesium, Acta Mater. 77 (2014) 28–42.
[22] Q. Yu, J. Wang, Y. Jiang, R.J. McCabe, C.N. Tomé, Co-zone $\{1\bar{0}12\}$ twin interaction in magnesium single crystal, Mater. Res. Lett. 2 (2) (2014) 82–88.
[23] Q. Yu, Y. Jiang, J. Wang, Tension-compression-tension tertiary twins in coarse-grained polycrystalline pure magnesium at room temperature, Philos. Mag. Lett. 95 (4) (2015) 194–201.
[24] S. Dong, Q. Yu, Y. Jiang, J. Dong, F. Wang, W. Ding, Cyclic deformation and fatigue of extruded ZK60 magnesium alloy with aging effects, Mater. Sci. Eng. A 615 (2014) 262–272.
[25] G. Wan, B.L. Wu, Y.D. Zhang, G.Y. Sha, C. Esling, Anisotropy of dynamic behavior of extruded AZ31 magnesium alloy, Mater. Sci. Eng. A 527 (2010) 2915–2924.
[26] L. Wu, S.R. Agnew, D.W. Brown, G.M. Stoica, B. Clausen, A. Jain, D.E. Fielden, P.K. Liaw, Internal stress relaxation and load redistribution during the twinning–detwinning–dominated cyclic deformation of a wrought magnesium alloy ZK60A, Acta Mater. 56 (2008) 3699–3707.
[27] M.R. Barnett, Z. Keshavarz, A.G. Beer, X. Ma, Non-Schmid behavior during secondary twinning in a polycrystalline magnesium alloy, Acta Mater. 56 (2008) 5–15.
[28] L. Jiang, J.J. Jonas, A.A. Luo, A.K. Sachdev, S. Godet, Twinning-induced softening in polycrystalline AM30 magnesium alloy at moderate temperatures, Scr. Mater. 54 (2006) 771–775.
[29] Y. Xiong, Microstructure damage evolution associated with cyclic deformation for extruded AZ31B magnesium alloy, Mater. Sci. Eng. A 675 (2016) 171–180.